ACS APPLIED NANO MATERIALS

www.acsanm.org Article

Geometrical Frustration and Defect Formation in Growth of Colloidal Nanoparticle Crystals on a Cylinder: Implications for Assembly of Chiral Nanomaterials

Nabila Tanjeem, William H. Wilkin, Daniel A. Beller, Chris H. Rycroft, and Vinothan N. Manoharan*

Cite This: *ACS Appl. Nano Mater.* 2021, 4, 10682−10691 Read Online

ACCESS | Metrics & More | Article Recommendations | Supporting Information

ABSTRACT: Using a combination of experiment and simulation, we study how two-dimensional (2D) crystals of colloidal nanoparticles grow on cylindrical substrates. The cylindrical geometry allows us to examine growth in the absence of Gaussian curvature but in the presence of a closure constraint—the requirement that a crystal loops back onto itself. In some cases, this constraint results in structures that have been observed previously in theory and nonequilibrium packing experiments: chiral crystals and crystals with linear defects known as "line slips". More generally, though, the structures we see differ from those that have been observed: the line slips are kinked and contain partial vacancies. We show that these structures arise because the cylinder changes how the crystal grows. After a crystal wraps around the cylinder and touches itself, it must grow preferentially along the cylinder axis. As a result, crystals with a chiral line slip tend to trap partial vacancies. Indeed, we find that line slips that are less aligned with the cylinder axis incorporate more partial vacancies on average than the ones that are more aligned. These results show that crystal growth on a cylinder is frustrated by the closure requirement, a finding that may shed some light on the assembly of biological nanosystems such as tobacco mosaic virus and might inform ways to fabricate chiral optical nanomaterials.

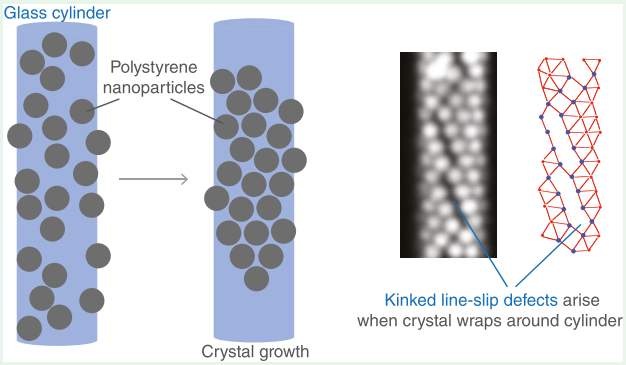

KEYWORDS: *colloidal crystallization, defects, frustration, crystal growth, self-assembly*

1. INTRODUCTION

The morphology of a crystal depends on how it nucleates and grows. Consequently, the structure of a real crystal often differs from an idealized equilibrium structure or ground state.[1] The connection between morphology and growth was first made by Steno[2] in the 17th century, long before the atomic theory. In the 1950s, Frank and co-workers[3] elucidated the relationships between crystal growth rates, thermal fluctuations, and atomic-scale structural features, including steps and defects. More recently, experiments on colloidal nanoparticles, which permit both structural details and growth[4−8] to be directly visualized, have led to a new understanding of crystal growth.

In particular, colloidal systems have revealed that curved substrates can fundamentally alter crystal growth. Most studies have focused on the role of the substrate's Gaussian curvature, the product of its two principal curvatures. Owing to Gaussian curvature, large two-dimensional (2D) crystals of colloidal spheres on a spherical substrate must incorporate topological defects.[9−15] When these defects are energetically costly, the crystal alters its growth to avoid them. For example, 2D crystals composed of particles with short-ranged attractions grow isotropically on a flat surface but anisotropically on a sphere.[16−19]

Here, we explore how a cylindrical substrate affects the growth of 2D crystals of colloidal nanoparticles. At first glance, one would not expect a cylindrical substrate to modify how such a crystal grows in the same way that a spherical substrate does: a cylinder has zero Gaussian curvature (because the curvature is zero along one direction); and hence, a crystal on a cylinder need not incorporate topological defects. Furthermore, a colloidal crystal on a cylinder—as opposed to one on a sphere—does not accrue stress as it grows. In other words, it would seem to have no way to "know" that it is on a curved surface.

However, this argument neglects one important feature of a cylindrical crystal: when it grows sufficiently large, it must meet itself, forming a closed loop. We show how this "closure constraint" affects how the crystal grows. On a plane, crystals do not have to contend with a closure constraint, and therefore, we

Received: July 26, 2021
Accepted: September 23, 2021
Published: October 11, 2021

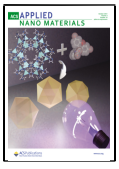

https://doi.org/10.1021/acsanm.1c02126
ACS Appl. Nano Mater. 2021, 4, 10682−10691

observe different patterns of growth and structure than are seen in planar crystals. On a sphere, crystals do contend with a closure constraint, and the effects of this closure constraint on spherical crystals have been studied in simulation.[20,21] But for a sphere, it is difficult to separate the effects of the global closure constraint from the local effects of Gaussian curvature, which leads to stress in a growing crystal. By examining a system with zero Gaussian curvature, we explore how closure alone might affect growth.

To this end, we first study the crystal morphologies and defects and then show what they reveal about growth. Most previous work on the morphologies of cylindrical crystals focuses only on idealized structures: densest packings and ground states. This problem dates back to (at the latest) the 1830s, with Louis and Auguste Bravais' mathematical analysis[22] of phyllotaxis, the arrangement of leaves around a plant stem. More recently, Pickett and co-workers[23] showed that for certain values of the size ratio r—the ratio of the cylinder diameter to sphere diameter—the densest packings of hard spheres *inside* a cylinder are chiral crystals. They also found that between size ratios corresponding to these commensurate crystals, the densest packings incorporate linear defects now known as "line slips", which consist of two parallel lines of spheres in which each sphere touches only five others. These defects have zero net Burgers vector.[24] Mughal and co-workers related these results to packings on the surface of a cylinder[25] (the phyllotactic problem) and showed that as the size ratio increases, the densest packings vary between achiral hexagonal packings, chiral hexagonal packings, and chiral hexagonal packings with line slips.[26] Later simulations by Wood and co-workers[24] showed that line slips can also occur in the ground states of particles with attractions.

Our study differs in two ways from these theoretical studies and from the few experimental studies of sphere packings inside cylinders.[27−30] First, we focus on how cylindrical crystals grow and not just on their structures. Second, the interactions between our nanoparticles are comparable to the thermal energy k_BT, so that nanoparticles in a growing crystal can rearrange. In these two respects, the crystallization process we study is much more similar to the self-assembly of a biological nanosystem than it is to phyllotactic growth. Thus, at the end of the paper, we compare our system to the tobacco mosaic virus (TMV), which also self-assembles at finite temperature and forms a cylindrical structure.

As we shall show, the closure constraint fundamentally alters the way the crystal grows, as evidenced by the random incorporation of a new type of defect (the partial vacancy) into the line slips. We find that crystals with highly helical line slips are more frustrated than crystals with less helical line slips. This result raises the question of how nanomaterials can be designed that avoid this frustration. The comparison with TMV suggests a potential approach to make chiral nanomaterials.

2. RESULTS AND DISCUSSION

2.1. Single Crystals Form on and Wrap around a Cylindrical Fiber. In our experimental system, 2D colloidal crystals self-assemble on the surface of a hard cylinder, driven by a short-ranged depletion interaction[33−35] between the particles and between the nanoparticles and the cylinder. We fabricate cylinders by simultaneously heating and pulling a silica optical fiber.[36−38] This method results in a tapered cylinder with a diameter d of a few micrometers and with a smooth surface for crystal growth (Figure 1a).

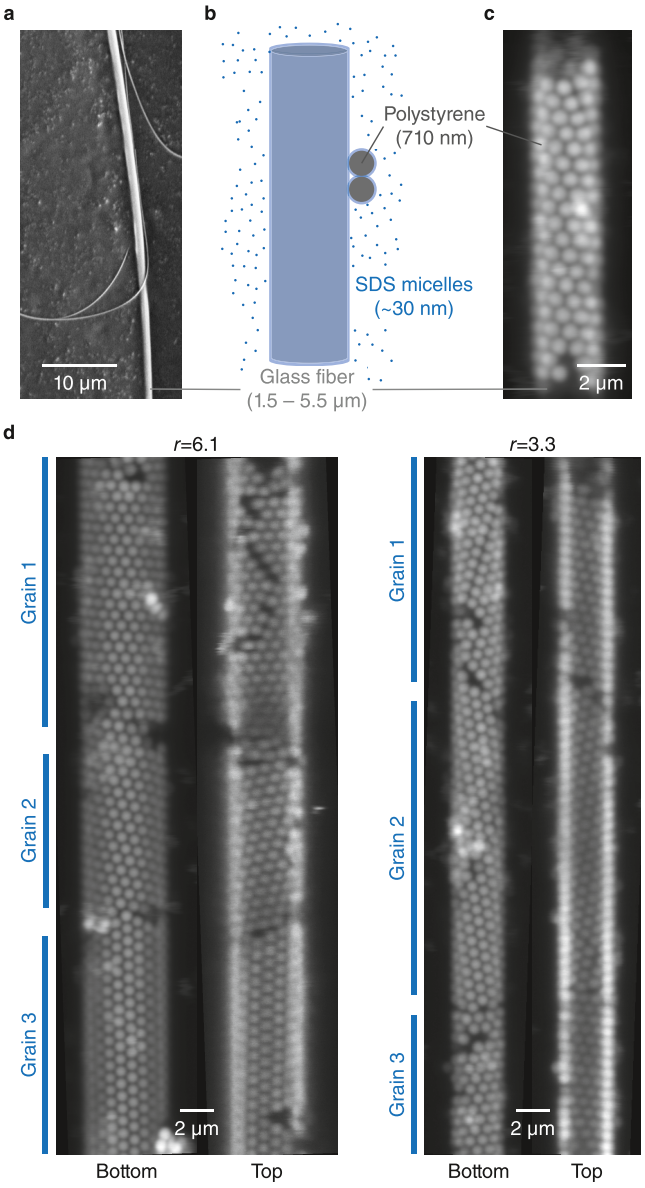

Figure 1. Formation of colloidal crystals on a cylinder. (a) Scanning electron micrograph of an optical fiber tapered from an original diameter of 125 μm to about 200 nm at its thinnest part. Both thick and thin segments in the image belong to the same fiber. We examine crystals that form where the fiber diameter is between 1.5 and 5.5 μm. (b) Polystyrene colloidal nanoparticles with an average diameter of 710 nm are attracted to the fiber through a depletion interaction mediated by SDS micelles with an effective diameter of 30 nm.[31,32] This effective diameter is larger than the physical diameter of 4 nm because it accounts for electrostatic interactions. The blue shaded regions denote the volume excluded to the micelles. We adjust the concentration of colloidal nanoparticles (0.25% w/v) and SDS (33.6−34 mM) in solution to prevent the formation of multiple crystal layers, large clusters of particles, or kinetic instabilities. (c) Projection of a stack of confocal microscope images of a colloidal crystal formed on the surface of a cylinder. (d) Confocal microscope images of crystals assembled on two cylinders with different size ratios r. Because the objective is below the cylinder, images of the top and sides of the cylinder are distorted by lensing through the glass fiber (see Figure S2 for details of experimental setup). The blue lines denote the approximate boundaries of different crystal grains that wrap around the cylinder. These grains are identified by the consistent chiral angle found on both sides of the cylinder.

https://doi.org/10.1021/acsanm.1c02126
ACS Appl. Nano Mater. 2021, 4, 10682−10691

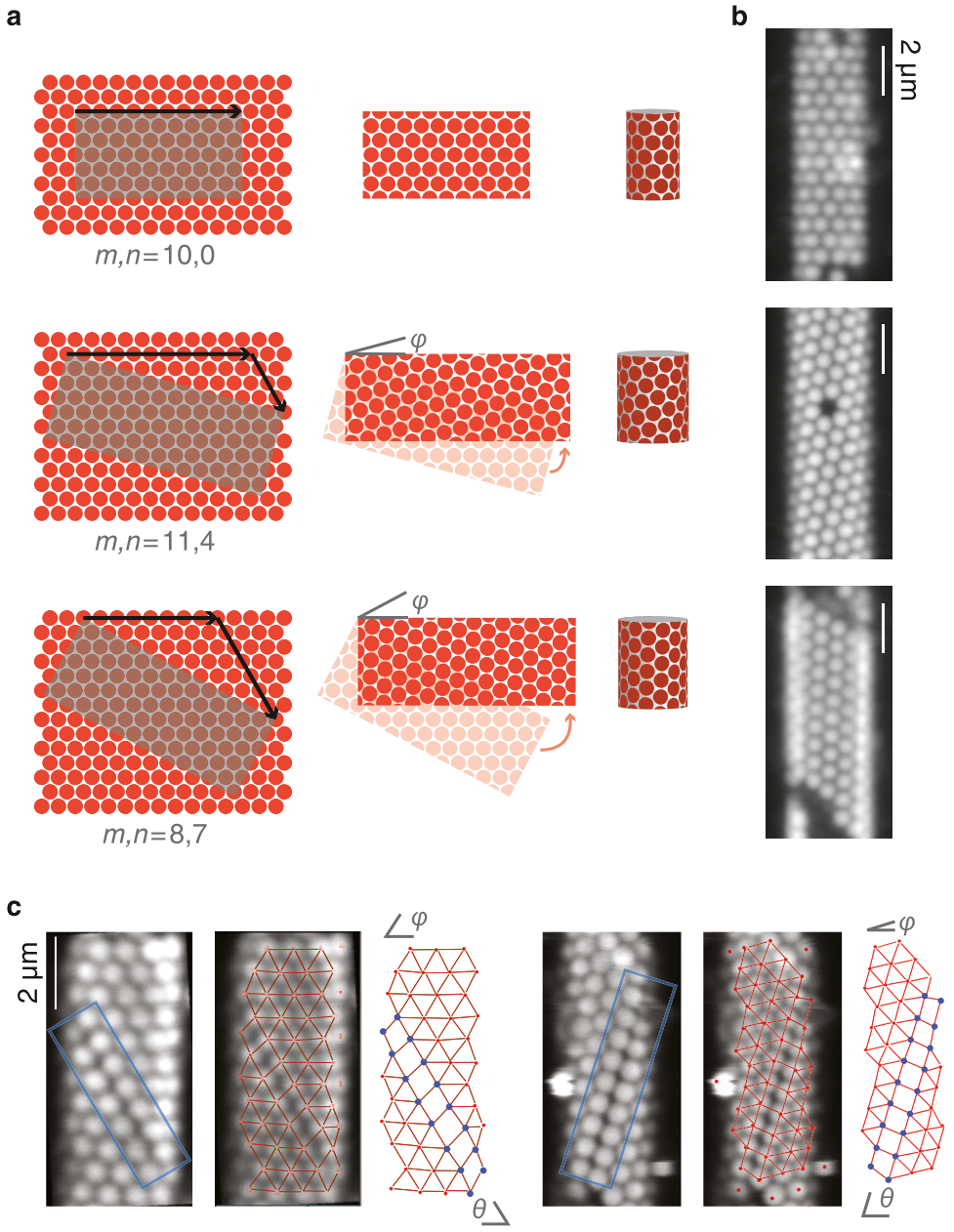

Figure 2. Some, but not all of the observed crystals, have structures corresponding to densest packings on a cylinder. (a) Diagrams showing the construction of commensurate cylindrical crystals. When the side length of the dark rectangle is commensurate with an integer linear combination (m,n) of the lattice vectors $\mathbf{v}_1$ and $\mathbf{v}_2$ (dark arrows show the vectors $m\mathbf{v}_1$ and $n\mathbf{v}_2$), the resulting segment of the lattice (middle column) can wrap perfectly around a cylinder with circumference $\|m\mathbf{v}_1 + n\mathbf{v}_2\|$. As shown in the middle and right columns, the integers m and n determine the chiral angle ϕ. An achiral crystal results from $(m,n) = (10,0)$, whereas chiral crystals result from (11,4) and (8,7). (b) Confocal microscope images of three crystals grown on the same tapered fiber. The chiral angles are $\phi = 0°$ (top), 16.3° (middle), and 27.6° (bottom). The resulting configurations are close to the corresponding diagrams in (a). (c) Confocal images and bond (interaction) networks of two line-slip defects (blue boxes) with different helicity. The helicity of a line slip is determined by the angle θ between the line slip and the azimuthal direction on the cylinder. Blue circles show the particles that form the line slip. Images of both sides of the cylinders shown in panels (b, c) are shown in Figure S7.

We introduce a depletion interaction between the polystyrene nanoparticles (diameter D = 710 nm) and between the nanoparticles and the cylinder using sodium dodecyl sulfate (SDS) micelles (Figure 1b). Because the interaction between nanoparticles is isotropic, a 2D crystal of such particles can bend freely and conform to the cylinder surface, which has no Gaussian curvature but does have nonzero mean curvature. The potential-well depth is a few k_BT (see Supporting Information), and the interaction range is approximately the effective diameter of the depletant micelles or about 4% of the polystyrene nanoparticle size at the SDS concentration we use (Figure 1b).[31,32] With such a weak and short-ranged attraction, isolated dislocations or disclinations do not occur.[17] Because only nanoparticles very close to one another interact, we refer to the attraction between two neighboring nanoparticles as a "bond." Furthermore, we choose the SDS concentration so that the crystals grow slowly and kinetic instabilities are avoided (Supporting Information).

Immediately after preparing the sample, we see multiple crystallites growing on the cylinder. In 3−5 h, the cylinder is

https://doi.org/10.1021/acsanm.1c02126
ACS Appl. Nano Mater. 2021, 4, 10682−10691

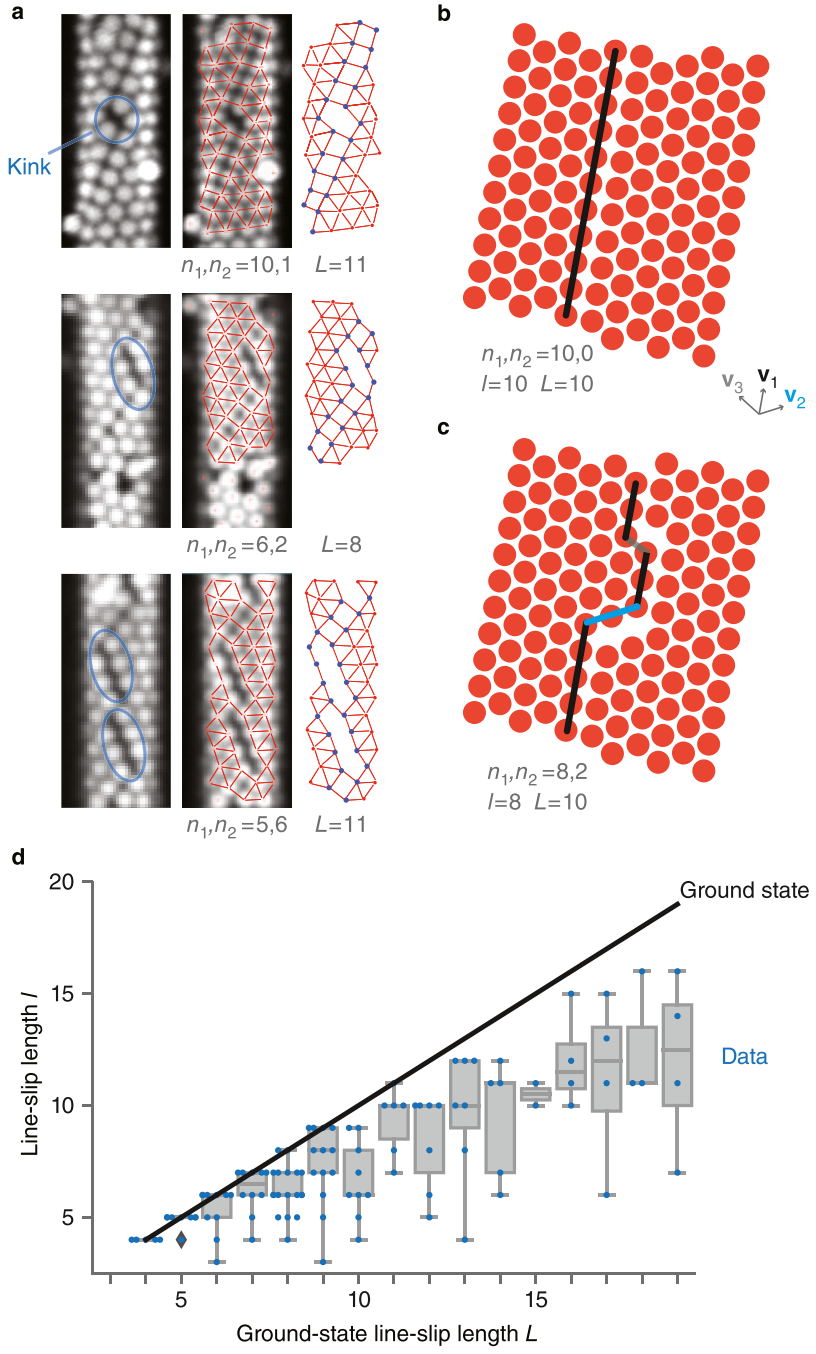

Figure 3. Most crystals with line-slip defects have kinks and are not ground-state structures. (a) Confocal images and bond networks of three kinked line-slip defects, with the kinks circled in blue. We characterize each defect by counting the number of steps (particle center-to-center distances) from its starting to ending point. n_1 is the number of steps taken along $\mathbf{v}_1$, the lattice direction aligned with the line slip, and n_2 along $\mathbf{v}_2$. Two parameters characterize the geometry: the line-slip length $l = n_1$, which is the number of particles in the line slip that have five neighbors, and the ground-state length $L = n_1 + n_2$, which is the length if all of the partial vacancies were to exit the line slip. Images of both sides of the cylinders are shown in Fig. S7. (**b**) Diagram of a line-slip defect in its ground state. $L = l$ because there are no kinks. (c) Diagram of a line-slip defect with kinks. Because of the kinks, $l < L$. (d) Plot of l as a function of L for ground states (black line) and experiment (blue dots). To find l from the experiment, we measure n_1 and n_2 from images of 116 crystals. The experimental data is shown as a box-and-whisker plot with data points in blue. The box extends from the lower to upper quartile, and the whiskers show the range of the data at each L.

almost entirely covered with crystallites (Figure 1c; for comparison, Figure S5 shows crystallization on a flat surface). To study the closure of individual crystallites, we limit our observations to size ratios $r = d/D$ between 2 and 6, in which case, multiple grains form along the length of the cylinder, each of which wraps completely around the cylinder (Figures 1d and S6). The cylinder is slightly tapered, allowing us to investigate the growth at different size ratios. But because the diameter of the fiber changes negligibly along a single grain, we can consider the substrate to be cylindrical rather than conical on the scale of the grain (Supporting Information).

2.2. At Long Times, Some Crystals Form Dense Packings but Most Contain Kinks. We first describe the structures of the cylindrical crystals that we observe at long times

https://doi.org/10.1021/acsanm.1c02126
ACS Appl. Nano Mater. 2021, 4, 10682−10691

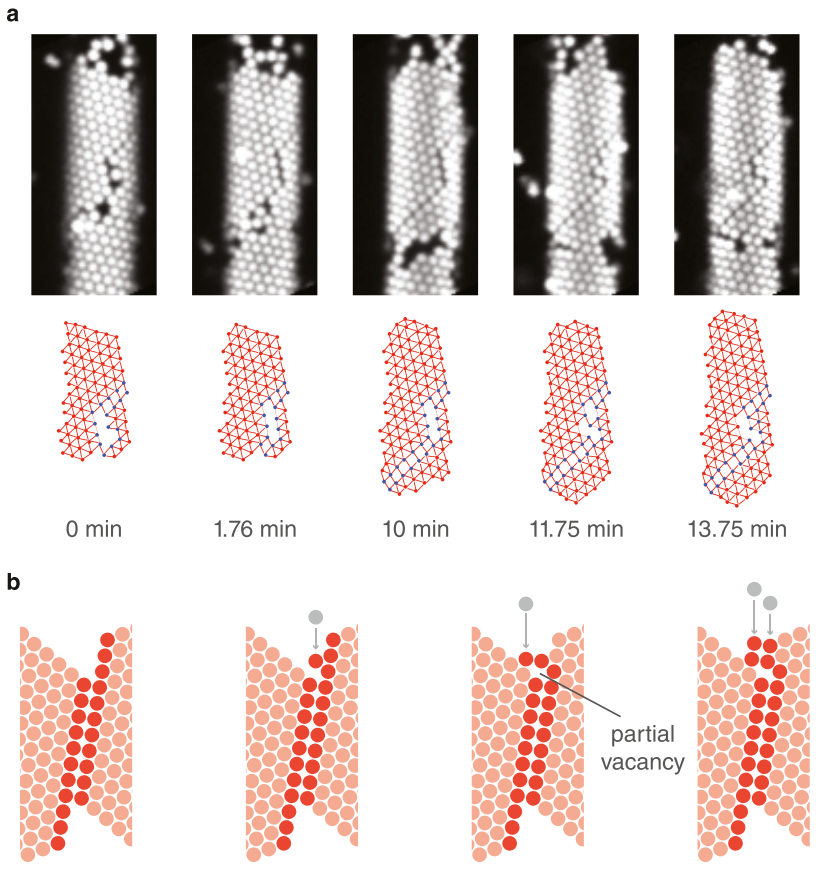

Figure 4. Kinked line slips form during the growth of the crystal. (a) Confocal images and bond networks showing the formation of a kinked line-slip defect. At 0 min, a line-slip defect begins to form when the crystal wraps around the cylinder. At 1.76 min, another line slip starts to form in parallel, leaving partial vacancies between the two. The line slips continue to grow until 10 min, after which we observe fluctuations in the kinked shape but not in the number of partial vacancies. Not all particles are shown in the bond network diagrams. (b) Diagrams illustrating a mechanism for kink formation. The growing line slip is shown by the dark red particles. In the second diagram, a particle that attaches to the crystal prevents the line slip from growing. In the third diagram, another particle attaches and traps a partial vacancy. In the fourth diagram, additional particles attach and continue the line slip, which is now kinked.

(several hours). We find that some, but not all, have structures corresponding to the densest packings predicted in previous theoretical studies: commensurate crystals and crystals with line slips. We discuss the geometry of these structures because it is essential for understanding the growth process and how it can lead to non-ground-state structures.

Some of the crystals we observe in our experiment are commensurate—the only defects being vacancies—and some of these are chiral. Mathematical models of phyllotaxis[25,39,40] show that commensurate crystals can appear for integer values of the chiral indices m and n (Figure 2a). These indices determine the size ratio and chiral angle of the crystal. We characterize the chiral angle of the observed crystals, which is easier to measure than m and n (Figure 2b). We find that crystals with different helicity can spontaneously assemble on different parts of the cylinder.

We also observe straight line-slip defects in some of the crystals (Figure 2c). Such defects have been observed previously in macroscopic systems[26,29] but not, to our knowledge, in a self-assembled system. They follow a helical path around the cylinder that is also parallel to one of the lattice vectors of the crystal.

The line-slip defects that we observe are stable for the duration of our experiments (up to 18 h), though vacancies do appear and disappear during that time. The stability is expected because line slips cannot disappear unless the crystal unwraps and rewraps, as shown in previous simulations and theoretical studies.[24,25] On a flat surface, defects similar to line slips can occur between two grains with similar orientations (Figure S8), but these defects disappear when the grains translate. On a cylinder, the line-slip defect occurs within the same grain, and thus translation along the line slip corresponds to a rotation of the crystal. However, rotating the crystal would change its circumference, which would require it to either penetrate the cylinder or detach from it, both of which are energetically prohibitive.

We find, however, that most crystals do not adopt ground-state structures, even at long times. Instead, they contain a new type of defect not previously seen in simulation or experiment: kinked line slips (Figure 3a). The kinks contain gaps that we call "partial vacancies" because they are smaller than a nanoparticle. We find that kinked line slips emerge in crystals with different chiral angles and with a variety of numbers of partial vacancies, as shown in Figure 3a. We characterize the different kinked structures using two length scales, as shown in Figure 3b,c. Quantification of these length scales for the observed structures (Figure 3d) illustrates two points. First, most of the line slips are kinked, and the proportion of line slips that are in the ground state decreases with increasing line-slip length. Second, for a given line-slip length, the number of partial vacancies can vary.

https://doi.org/10.1021/acsanm.1c02126
ACS Appl. Nano Mater. 2021, 4, 10682−10691

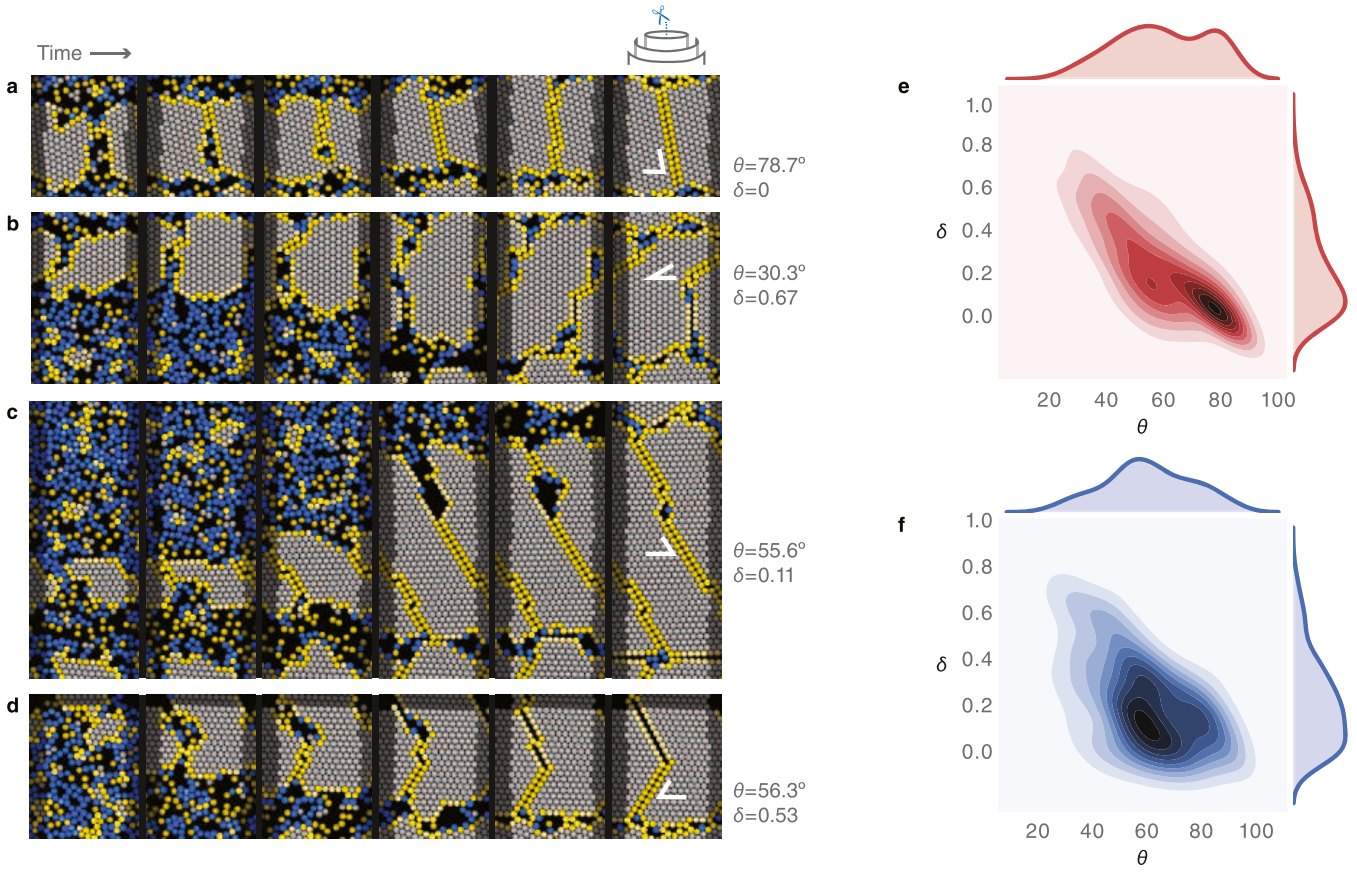

Figure 5. Line slips that are more aligned with the cylinder axis are less kinked. (a–d) Renderings of the simulated growth of four crystals with line slips. In each image, the crystal is shown cut and unwrapped, such that the entire circumference of the cylinder (same for all four crystals) is visible. The line-slip angle θ and parameter $\delta = (L - l)/L$ are shown at right for each crystal, and particles in the line slip and grain boundaries are shown in yellow. In (a), the line slip is nearly aligned with the cylinder axis. It forms kinks but eventually rearranges into a straight line slip. In (b), the line slip makes a larger angle with the axis. The crystal, however, grows preferentially in the axial direction and consequently traps partial vacancies, resulting in a larger value of δ. In (c) and (d), the line slips have angles between those of (a) and (b), and their values of δ also lie between those of (a) and (b). (e) Contour plot showing probability distribution (kernel density estimate) of kinked line-slip defects as a function of δ and θ for 79 simulated crystals with fixed r. (f) Same type of plot as (e) but showing data from 116 crystals found in the experiment with varying r. The correlation coefficient in the experiment (−0.49) is smaller than that of simulation (−0.77), likely because the experimental data are not taken at a single size ratio. The data points used to create the kernel density estimates in panels (e, f) are shown in Figure S12.

This variation shows that the partial vacancies do not affect the commensurability of the crystal with the cylindrical constraint. In fact, kinked line slips can, in principle, convert to straight line slips when partial vacancies move into the grain boundaries—or, equivalently, when multiple nanoparticles move in a direction parallel to the line slip. Such a relaxation does not require a change in cylinder circumference; instead, the excess void space can be absorbed by the grain boundaries. Thus, a kink can be viewed as an excitation of a straight line slip. Kinked line slips would therefore not have been observed in previous simulations on cylindrical crystals[24] that examined only the ground states.

2.3. Kinked Line Slips Form during Growth. Having shown that defects arise that do not change the commensurability constraint, we now turn to what these defects reveal about the growth process. To understand why the kinked line slips occur so frequently in our experiments, we watch line slips form in the experiment (Figure 4a and Movie S1). We find that kinked line slips tend to form when two parallel line slips grow, trapping partial vacancies in between. These observations suggest a mechanism for the formation of partial vacancies (Figure 4b).

We also find that once formed, most kinked defects do not relax into straight line slips on the timescale of the experiment (Figure S9), although the kinks and grain boundaries do fluctuate (Figure S10). Hence, in contrast to crystals that close without a line slip (Figure S11 and Movie S2), crystals with kinked line slips appear to result when partial vacancies are kinetically trapped during crystal growth. Brownian-dynamics simulations of particles interacting on a cylinder through a short-range potential that approximates the experimental depletion attraction (Supporting Information and Movie S3) show that kinks arise during growth and not afterward (Figure 5a–d and Movie S4).

The observation that these new defects arise during growth is the first clue that the cylindrical geometry affects the growth process itself. The second clue is that the parameter $\delta = (L - l)/L$, the number of partial vacancies per unit length of the total defect, is inversely correlated with the line-slip angle θ in both simulation (Figure 5e) and experiment (Figure 5f). Thus, line slips that are less aligned with the cylinder axis have more partial vacancies on average. This result was unexpected to us because the partial vacancies neither reduce the energy of the crystal nor

https://doi.org/10.1021/acsanm.1c02126
ACS Appl. Nano Mater. 2021, 4, 10682−10691

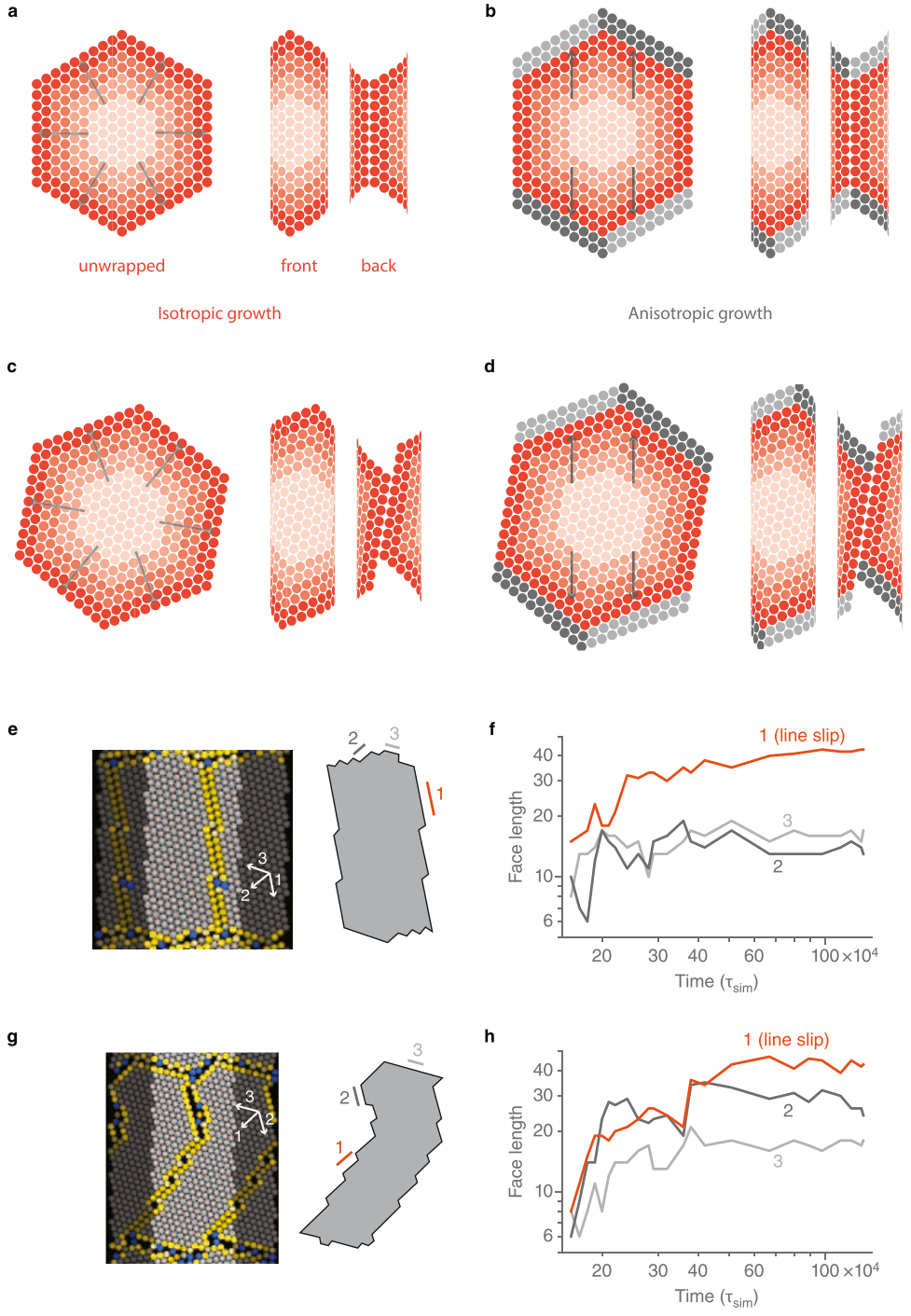

Figure 6. Kinks result from anisotropic growth after a crystal meets itself. (a) Illustrations of a crystal growing on a cylinder. Darker colors correspond to the later stages of growth. The crystal grows isotropically until it wraps and meets itself, forming a line slip. (b) The crystal must then grow along the cylinder axis. Gray circles indicate particles that attach to the two exposed faces of the crystal to continue the line slip. (c, d), Same as (a) and (b), but for a line slip that is less vertical. For the line slip to remain straight, the growth on the light and dark gray faces must be the same. But because these two faces make different angles with the average growth direction (along the axis), partial vacancies can become trapped by the mechanism of Figure 4b. (e) Rendering of a nearly vertical line slip ($\theta \approx 80°$) found in simulation. Diagram at the right shows the area of the crystal (shaded region) and three faces. (f) Lengths of the three faces as a function of time. The lengths are comparable until $2 \times 10^5\ \tau_{sim}$ (where $\tau_{sim} = 180$ ms), at which point face 1 (aligned with the line slip and closely aligned with the crystal axis) starts to dominate. (g, h), Same as (e) and (f), but for a less vertical line slip ($\theta \approx 45°$). Because face 2 is nearly aligned with the cylinder axis, it competes with face 1, and the line slip becomes kinked.

do they change the commensurability of the crystal with its substrate.

2.4. Cylindrical Geometry Affects the Growth Process. We make sense of the negative correlation between the line-slip angle and the density of partial vacancies as follows. On a flat plane, near equilibrium, a crystalline grain grows isotropically. The same should be true of a crystal on a cylinder until the grain wraps around the cylinder and the crystal touches itself. At this point, growth along the azimuthal direction of the cylinder is hindered, and the flux of particles arriving at the crystal is no

https://doi.org/10.1021/acsanm.1c02126
ACS Appl. Nano Mater. 2021, 4, 10682−10691

longer isotropic. A line slip that is aligned with the cylinder axis can continue to grow without kinks after it meets itself (Figure 6a) because of symmetry: the two other faces of the crystal make the same angle with the cylinder axis, and therefore particles can attach to them at the same rates (Figure 6b). By contrast, a line slip that is less aligned with the cylinder axis faces a challenge when it meets itself (Figure 6c) because the other two faces make different angles with the line slip. Continuing the line slip without defects requires particles to attach to both faces at the same rates (Figure 6d), but the broken symmetry makes this scenario unlikely: the larger the angle between the cylinder axis and the face corresponding to the line slip, the higher the probability that particles land on this face and trap partial vacancies by the mechanism of Figure 4b.

Although this simple picture of the growth dynamics ignores effects such as diffusion of partial vacancies, it does describe the dynamics seen in simulations. To quantify these dynamics, we measure the lengths of all three faces of the crystal as a function of time. These lengths are related to the rates at which particles attach to faces—for example, the length of face 1 increases when particles attach to faces 2 and 3—but are easier to measure. We find that for a crystal with a line slip that is nearly aligned with the cylinder axis (Figure 6e and Movie S5), the lengths of the faces are approximately the same at short times, indicating isotropic growth (Figure 6f). At longer times, the growth becomes anisotropic, with the face aligned with the line slip (face 1), growing much longer than the other two (faces 2 and 3). The disparity between the length of face 1 and the lengths of faces 2 and 3 indicates that relatively few particles attach *to* face 1. As a result, the crystal incorporates few partial vacancies. A crystal with a line slip that is misaligned with the cylinder axis (Figure 6g and Movie S6) also shows approximately isotropic growth at short times (Figure 6h), but at longer times, the face aligned with the line slip (face 1) competes with face 2, which is more closely aligned with the cylinder axis. As a result, the crystal traps several partial vacancies.

2.5. Conclusions. We have shown how the closure constraint changes the growth of a crystal composed of nanoparticles on a cylindrical substrate. The crystal grows approximately isotropically (as shown by our simulations) until it meets itself, at which point it must grow preferentially along the cylinder axis. As a result, the larger the angle between the line slip and the cylinder axis, the more partial vacancies the crystal incorporates.

These results have both fundamental and practical implications for nanomaterials. From the fundamental perspective, they show that a closure constraint alone can frustrate crystal growth. This is a different type of geometrical frustration[15,41] from the more well-studied form arising from Gaussian curvature.[41,42] It does not occur in planar 2D crystals, where there is no closure constraint. It manifests only when the crystal size becomes comparable to the circumference, which is why the defects, partial vacancies, occur only where the crystal meets itself.

From a practical perspective, our results show that some ground-state cylindrical crystals are harder to make than others. In particular, it is difficult to grow a dense crystal having a line slip that is tightly wound about the axis, owing to the mismatch between the line slip and the growth direction. Thus, self-assembly may be an inefficient way to make certain chiral nanomaterials, which have applications in sensors[43] and optical metamaterials.[44] Indeed, existing self-assembly routes to such nanostructures rely on templates such as TMV capsids[44,45] and DNA origami rods[46] that guide nanoparticles into a prescribed helicity. An interesting question is whether there are conditions under which nonspecific substrates, like the fibers we use, can template the formation of large, single crystals with prescribed helicity and line-slip structure.

To address this question, it is useful to examine self-assembled cylindrical nanosystems that are not frustrated. Single-wall carbon nanotubes,[47,48] for example, can adopt diameters corresponding to commensurate crystals, and microtubules can adopt straight line slips (called "seams"[49]) because these structures do not form around a cylindrical template. However, in systems like ours, the nanoparticles must satisfy the closure constraint while simultaneously adhering to a template. There are several systems in biology that face a similar set of competing constraints.[40]

Of these, the tobacco mosaic virus (TMV) has a particularly interesting way to satisfy both the closure and adhesion constraints. The coat proteins of TMV self-assemble into a cylindrical capsid around the viral RNA, even *in vitro*[50]—indeed, the TMV capsid is the structure that first inspired the term "self-assembly".[51] However, the assembly pathway differs from that in our system. The coat proteins first assemble into disks,[52] and a single site on the RNA nucleates the formation of the cylindrical capsid from these disks.[53] During nucleation and assembly, the disks "dislocate",[52,54] or shear, to form helical structures, thereby reducing their diameter and adhering to the RNA.

Thus, in TMV, the proteins first satisfy the closure constraint by forming disks and afterward adhere to the RNA template. They maintain the closure constraint during the dislocating process. By contrast, the nanoparticles in our system first adhere to the template, then form crystals that must close. Our results show that even a single crystal can be frustrated by the closure constraint; therefore, the control over nucleation that the RNA provides may not be as important to eliminating frustration in TMV as the sequential nature of the assembly. This assembly pathway might have evolved in part to prevent the formation of line slips or partial vacancies that would expose the RNA to degradation by nucleases. There are, of course, other differences between our system and TMV. For example, the interactions between coat proteins are longer-ranged in TMV, which might help vacancies exit by allowing dislocations to form and glide helically to relax stresses.[55,56] But the most striking difference is that the assembly is staged in a way that allows for both closure and adhesion. Engineering a similarly staged process may permit the directed self-assembly of nanoparticles into prescribed chiral crystals with high yield.

Another question for future work is why the kinked line slips take so long to relax. Understanding their relaxation dynamics—and how those dynamics slow with increasing interaction strength and line-slip size—might reveal more about the relatively simple but unexplored form of geometrical frustration imposed by a cylindrical surface.

3. METHODS

See Supporting Information for all details of the experimental and computational methods.

■ ASSOCIATED CONTENT

Supporting Information

The Supporting Information is available free of charge at https://pubs.acs.org/doi/10.1021/acsanm.1c02126.

https://doi.org/10.1021/acsanm.1c02126
ACS Appl. Nano Mater. 2021, 4, 10682−10691

Supporting information document: includes detailed Materials and Methods, Figures S1 to S12, and Table S1 (PDF)

Confocal images showing a crystal on a cylinder forming a kinked line-slip defect. Snapshots of this movie are shown in Figure 4 of the manuscript (Movie S1) (MOV)

Confocal images showing a crystal on a cylinder without any defects. Snapshots of this movie are presented in Figure S11 (Movie S2) (MOV)

Rendering of crystal growth on a cylinder from a Brownian-dynamics simulation. The four images are of the same cylinder taken from four azimuthal angles at 90° intervals (Movie S3) (MOV)

Rendering of crystal growth on a cylinder from a Brownian-dynamics simulation, showing the cylinder cut and unwrapped. Snapshots of this movie are presented in Figure 5 of the manuscript (Movie S4) (MOV)

Rendering of Brownian-dynamics simulation showing the growth of a crystal with a line slip that is nearly aligned with the cylinder axis (Movie S5) (MOV)

Rendering of Brownian-dynamics simulation showing the growth of a crystal with a line slip that is misaligned with the cylinder axis (Movie S6) (MOV)

AUTHOR INFORMATION

Corresponding Author

Vinothan N. Manoharan − *Harvard John A. Paulson School of Engineering and Applied Sciences, Harvard University, Cambridge, Massachusetts 02138, United States; Department of Physics, Harvard University, Cambridge, Massachusetts 02138, United States;* orcid.org/0000-0003-0370-6095; Email: vnm@seas.harvard.edu

Authors

Nabila Tanjeem − *Harvard John A. Paulson School of Engineering and Applied Sciences, Harvard University, Cambridge, Massachusetts 02138, United States*

William H. Wilkin − *Department of Physics, Harvard University, Cambridge, Massachusetts 02138, United States*

Daniel A. Beller − *Department of Physics, University of California, Merced, California 95343, United States*

Chris H. Rycroft − *Harvard John A. Paulson School of Engineering and Applied Sciences, Harvard University, Cambridge, Massachusetts 02138, United States; Computational Research Division, Lawrence Berkeley Laboratory, Berkeley, California 94720, United States*

Complete contact information is available at: https://pubs.acs.org/10.1021/acsanm.1c02126

Notes

The authors declare no competing financial interest.

ACKNOWLEDGMENTS

The authors thank Smarak Maity, Amirhassan Shams-Ansari, and Michael Burek for help with the fabrication of the cylinders; Guangnan Meng and Sandra Nakasone for help with experimental protocols; and Frans Spaepen, Adil Mughal, David Nelson, Michael Moshe, Rodrick Kuate Defo, and L. Mahadevan for helpful discussions. This work was supported by the Harvard MRSEC under the National Science Foundation Grant Nos. DMR-1420570 and DMR-2011754. C.H.R. was partially supported by the Applied Mathematics Program of the U.S. DOE Office of Science Advanced Scientific Computing Research under contract number DE-AC02-05CH11231.

REFERENCES

(1) Sunagawa, I. Growth and Morphology of Crystals. *Forma* **1999**, *14*, 147−166.

(2) Steno, N. *De solido intra solidum naturaliter contento dissertationis prodromus*; 1669; English translation by John Garrett Winter, "The prodromus of Nicolaus Steno's dissertation concerning a solid body enclosed by process of nature within a solid; an English version with an introduction and explanatory notes " MacMillan: London, 1916.

(3) Burton, W. K.; Cabrera, N.; Frank, F. C. The growth of crystals and the equilibrium structure of their surfaces. *Philos. Trans. R. Soc., A* **1951**, *243*, 299−358.

(4) Palberg, T. Colloidal crystallization dynamics. *Curr. Opin. Colloid Interface Sci.* **1997**, *2*, 607−614.

(5) Skjeltorp, A. T. Visualization and characterization of colloidal growth from ramified to faceted structures. *Phys. Rev. Lett.* **1987**, *58*, 1444−1447.

(6) de Villeneuve, V. W. A.; Dullens, R. P. A.; Aarts, D. G. A. L.; Groeneveld, E.; Scherff, J. H.; Kegel, W. K.; Lekkerkerker, H. N. W. Colloidal Hard-Sphere Crystal Growth Frustrated by Large Spherical Impurities. *Science* **2005**, *309*, 1231−1233.

(7) Savage, J. R.; Dinsmore, A. D. Experimental Evidence for Two-Step Nucleation in Colloidal Crystallization. *Phys. Rev. Lett.* **2009**, *102*, 198302.

(8) Ganapathy, R.; Buckley, M. R.; Gerbode, S. J.; Cohen, I. Direct Measurements of Island Growth and Step-Edge Barriers in Colloidal Epitaxy. *Science* **2010**, *327*, 445−448.

(9) Schreiner, W.; Kratky, K. W. Computer simulation of hard-disc packings with spherical boundary conditions. *J. Chem. Soc., Faraday Trans. 2* **1982**, *78*, 379−389.

(10) Bowick, M.; Cacciuto, A.; Nelson, D. R.; Travesset, A. Crystalline Order on a Sphere and the Generalized Thomson Problem. *Phys. Rev. Lett.* **2002**, *89*, No. 185502.

(11) Bausch, A. R.; Bowick, M. J.; Cacciuto, A.; Dinsmore, A. D.; Hsu, M. F.; Nelson, D. R.; Nikolaides, M. G.; Travesset, A.; Weitz, D. A. Grain Boundary Scars and Spherical Crystallography. *Science* **2003**, *299*, 1716−1718.

(12) Lipowsky, P.; Bowick, M. J.; Meinke, J. H.; Nelson, D. R.; Bausch, A. R. Direct visualization of dislocation dynamics in grain-boundary scars. *Nat. Mater.* **2005**, *4*, 407.

(13) García, N. A.; Register, R. A.; Vega, D. A.; Gómez, L. R. Crystallization dynamics on curved surfaces. *Phys. Rev. E* **2013**, *88*, No. 012306.

(14) Guerra, R. E.; Kelleher, C. P.; Hollingsworth, A. D.; Chaikin, P. M. Freezing on a sphere. *Nature* **2018**, *554*, 346−350.

(15) Grason, G. M. Perspective Geometrically frustrated assemblies. *J. Chem. Phys.* **2016**, *145*, No. 110901.

(16) Schneider, S.; Gompper, G. Shapes of crystalline domains on spherical fluid vesicles. *Europhys. Lett.* **2005**, *70*, 136−142.

(17) Meng, G.; Paulose, J.; Nelson, D. R.; Manoharan, V. N. Elastic Instability of a Crystal Growing on a Curved Surface. *Science* **2014**, *343*, 634−637.

(18) Vega, D. A.; Lorenzana, J.; Gómez, L. R.; García, N. A.; Vitelli, V. Phase nucleation in curved space. *Nat. Commun.* **2015**, *6*, No. 6856.

(19) Köhler, C.; Backofen, R.; Voigt, A. Stress Induced Branching of Growing Crystals on Curved Surfaces. *Phys. Rev. Lett.* **2016**, *116*, No. 135502.

(20) Luque, A.; Reguera, D.; Morozov, A.; Rudnick, J.; Bruinsma, R. Physics of shell assembly: Line tension, hole implosion, and closure catastrophe. *J. Chem. Phys.* **2012**, *136*, No. 184507.

(21) Michaels, T. C. T.; Bellaiche, M. M. J.; Hagan, M. F.; Knowles, T. P. J. Kinetic constraints on self-assembly into closed supramolecular structures. *Sci. Rep.* **2017**, *7*, No. 12295.

(22) Bravais, L.; Bravais, A. Essai sur la disposition des feuilles curviséries. *Ann. Sci. Nat., Bot.* **1837**, *7*, 42−110.

(23) Pickett, G. T.; Gross, M.; Okuyama, H. Spontaneous Chirality in Simple Systems. *Phys. Rev. Lett.* **2000**, *85*, 3652−3655.

(24) Wood, D. A.; Santangelo, C. D.; Dinsmore, A. D. Self-assembly on a cylinder: a model system for understanding the constraint of commensurability. *Soft Matter* **2013**, *9*, 10016.
(25) Mughal, A.; Chan, H. K.; Weaire, D. Phyllotactic Description of Hard Sphere Packing in Cylindrical Channels. *Phys. Rev. Lett.* **2011**, *106*, No. 115704.
(26) Mughal, A.; Chan, H. K.; Weaire, D.; Hutzler, S. Dense packings of spheres in cylinders: Simulations. *Phys. Rev. E* **2012**, *85*, No. 051305.
(27) Lohr, M. A.; Alsayed, A. M.; Chen, B. G.; Zhang, Z.; Kamien, R. D.; Yodh, A. G. Helical packings and phase transformations of soft spheres in cylinders. *Phys. Rev. E* **2010**, *81*, No. 040401.
(28) Wu, G.; Cho, H.; Wood, D. A.; Dinsmore, A. D.; Yang, S. Confined Assemblies of Colloidal Particles with Soft Repulsive Interactions. *J. Am. Chem. Soc.* **2017**, *139*, 5095−5101.
(29) Winkelmann, J.; Haffner, B.; Weaire, D.; Mughal, A.; Hutzler, S. Simulation and observation of line-slip structures in columnar structures of soft spheres. *Phys. Rev. E* **2017**, *97*, No. 059902.
(30) Ouhajji, S.; van Ravensteijn, B. G. P.; Fernández-Rico, C.; Lacina, K. S.; Philipse, A. P.; Petukhov, A. V. Wet-Chemical Synthesis of Chiral Colloids. *ACS Nano* **2018**, *12*, 12089−12095.
(31) Iracki, T. D.; Beltran-Villegas, D. J.; Eichmann, S. L.; Bevan, M. A. Charged Micelle Depletion Attraction and Interfacial Colloidal Phase Behavior. *Langmuir* **2010**, *26*, 18710−18717.
(32) Tulpar, A.; Subramanian, V.; Ducker, W. Decay Lengths of Double-Layer Forces in Solutions of Partly Associated Ions. *Langmuir* **2001**, *17*, 8451−8454.
(33) Asakura, S.; Oosawa, F. On Interaction between Two Bodies Immersed in a Solution of Macromolecules. *J. Chem. Phys.* **1954**, *22*, 1255−1256.
(34) Asakura, S.; Oosawa, F. Interaction between particles suspended in solutions of macromolecules. *J. Polym. Sci.* **1958**, *33*, 183−192.
(35) Binder, K.; Virnau, P.; Statt, A. Perspective: The Asakura Oosawa model: A colloid prototype for bulk and interfacial phase behavior. *J. Chem. Phys.* **2014**, *141*, No. 140901.
(36) Tong, L.; Gattass, R. R.; Ashcom, J. B.; He, S.; Lou, J.; Shen, M.; Maxwell, I.; Mazur, E. Subwavelength-diameter silica wires for low-loss optical wave guiding. *Nature* **2003**, *426*, 816−819.
(37) Tong, L.; Lou, J.; Ye, Z.; Svacha, G. T.; Mazur, E. Self-modulated taper drawing of silica nanowires. *Nanotechnology* **2005**, *16*, 1445−1448.
(38) Tong, L.; Mazur, E. Glass nanofibers for micro- and nano-scale photonic devices. *J. Non-Cryst. Solids* **2008**, *354*, 1240−1244.
(39) van Iterson, G. *Mathematische und mikroskopisch-anatomische Studien über Blattstellungen nebst Betrachtungen über den Schalenbau der Miliolinen*; Fischer: Jena, 1907.
(40) Erickson, R. O. Tubular Packing of Spheres in Biological Fine Structure. *Science* **1973**, *181*, 705−716.
(41) Sadoc, J.-F.; Mosseri, R. *Geometrical Frustration; Collection Alea-Saclay: Monographs and Texts in Statistical Physics*; Cambridge University Press: Cambridge, 1999.
(42) Bowick, M. J.; Giomi, L. Two-dimensional matter: order, curvature and defects. *Adv. Phys.* **2009**, *58*, 449−563.
(43) Cecconello, A.; Besteiro, L. V.; Govorov, A. O.; Willner, I. Chiroplasmonic DNA-based nanostructures. *Nat. Rev. Mater.* **2017**, *2*, No. 17039.
(44) Kobayashi, M.; Tomita, S.; Sawada, K.; Shiba, K.; Yanagi, H.; Yamashita, I.; Uraoka, Y. Chiral meta-molecules consisting of gold nanoparticles and genetically engineered tobacco mosaic virus. *Opt. Express* **2012**, *20*, 24856−24863.
(45) Dujardin, E.; Peet, C.; Stubbs, G.; Culver, J. N.; Mann, S. Organization of Metallic Nanoparticles Using Tobacco Mosaic Virus Templates. *Nano Lett.* **2003**, *3*, 413−417.
(46) Kuzyk, A.; Schreiber, R.; Fan, Z.; Pardatscher, G.; Roller, E.-M.; Högele, A.; Simmel, F. C.; Govorov, A. O.; Liedl, T. DNA-based self-assembly of chiral plasmonic nanostructures with tailored optical response. *Nature* **2012**, *483*, 311−314.
(47) Iijima, S.; Ichihashi, T. Single-shell carbon nanotubes of 1-nm diameter. *Nature* **1993**, *363*, 603−605.
(48) Bethune, D. S.; Kiang, C. H.; Vries, M. S. d.; Gorman, G.; Savoy, R.; Vazquez, J.; Beyers, R. Cobalt-catalysed growth of carbon nanotubes with single-atomic-layer walls. *Nature* **1993**, *363*, 605−607.
(49) Kikkawa, M.; Ishikawa, T.; Nakata, T.; Wakabayashi, T.; Hirokawa, N. Direct visualization of the microtubule lattice seam both in vitro and in vivo. *J. Cell Biol.* **1994**, *127*, 1965−1971.
(50) Fraenkel-Conrat, H.; Williams, R. C. Reconstitution of Active Tobacco Mosaic Virus from Its Inactive Protein and Nucleic Acid Components. *Proc. Natl. Acad. Sci. U.S.A.* **1955**, *41*, 690−698.
(51) Caspar, D. L. D.; Klug, A. Physical Principles in the Construction of Regular Viruses. *Cold Spring Harbor Symp. Quant. Biol.* **1962**, *27*, 1−24.
(52) Butler, P. J. G. Assembly of Tobacco Mosaic Virus Particle. *Nature* **1971**, *233*, 25−27.
(53) Butler, P. J. G. Self−assembly of tobacco mosaic virus: the role of an intermediate aggregate in generating both specificity and speed. *Philos. Trans. R. Soc., B* **1999**, *354*, 537−550.
(54) Klug, A. The Tobacco Mosaic Virus Particle: Structure and Assembly. *Philos. Trans. R. Soc. London, Ser. B.* **1999**, *354*, 531−535.
(55) Harris, W. F. Dislocations in Tobacco Mosaic Virus. *Nature* **1972**, *240*, 294−297.
(56) Beller, D. A.; Nelson, D. R. Plastic deformation of tubular crystals by dislocation glide. *Phys. Rev. E* **2016**, *94*, No. 033004.

https://doi.org/10.1021/acsanm.1c02126
ACS Appl. Nano Mater. 2021, 4, 10682−10691